



Improved cycle stability of Fe–air solid state oxide rechargeable battery using LaGaO₃-based oxide ion conductor



Atsushi Inoishi ^a, Takaaki Sakai ^b, Young Wan Ju ^a, Shintaro Ida ^{a,c}, Tatsumi Ishihara ^{a,c,*}

^a Department of Applied Chemistry, Faculty of Engineering, Kyushu University, Japan

^b Center for Molecular Systems, Kyushu University, 744 Motooka, Nishi-ku, Fukuoka 819-0395, Japan

^c International Institute for Carbon Neutral Energy Research (WPI-I2CNER), 744 Motooka, Nishi-ku, Fukuoka 819-0395, Japan

HIGHLIGHTS

- Effect of operating temperature of an Fe–air rechargeable battery was studied.
- Lower operating temperature contributed to the higher performance of the battery.
- 30 cycles with high energy density and energy efficiency could be observed at 773 K.
- Suppressed aggregation of anode and Fe powder contributed to the high performance.

ARTICLE INFO

Article history:

Received 21 August 2013

Received in revised form

19 March 2014

Accepted 25 March 2014

Available online 8 April 2014

Keywords:

Fe–air rechargeable battery

Oxide ion conductor

Operation temperature

LaGaO₃ based oxide

ABSTRACT

The effect of operating temperature on the discharge potential and cycle stability of an Fe–air solid oxide rechargeable battery was studied. An Fe–air cell operated at 773 K exhibited the highest discharge potential (1.07 V) and high cycle stability with a current density of 5 mA cm⁻². The high discharge potential at lower operating temperatures is due to aggregation of the anode and Fe powder being suppressed. The high redox cycle stability of the Ni–Fe-based anode at 773 K is explained by the small volume change with suppressed aggregation under low-temperature operation. Electrochemical charge–discharge measurements at 773 K revealed excellent cycle stability for 30 cycles with a high energy density (round trip efficiency >80%).

© 2014 Elsevier B.V. All rights reserved.

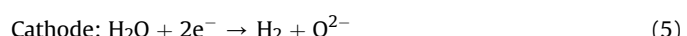
1. Introduction

Rechargeable batteries with extremely large capacity are in strong demand as energy storage devices for electric power grid applications and for use in electric vehicles (EVs) [1]. The metal–air battery is attracting much interest due to its large theoretical energy density because the cathode active material is not necessary for energy storage [2–6]. Among the various metal–air batteries, the Fe–air battery has the advantage of large capacity, in addition to Fe being environmentally compatible and cheap. Recently, Xu et al. reported a combination of solid oxide fuel cell (SOFC) technology with a ZrO₂ based electrolyte and the redox of Fe through a H₂/H₂O redox mediator [7,8]. We have proposed the application of LaGaO₃ or ZrO₂ based oxide ion conducting

electrolytes to metal–air batteries [9–13]. Discharge of the Fe–air battery proceeds according to the following electrode reactions:



In the discharge, Fe powder can react with H₂O generated in the cell to form H₂, which can be used for the fuel for discharge. On the other hand, electrochemical charge reaction is just opposite reaction, and therefore, charge proceeds according to the following electrode reactions:



* Corresponding author. Department of Applied Chemistry, Faculty of Engineering, Kyushu University, 744 Motooka, Nishi-ku, Fukuoka 819-0395, Japan. Fax: +81 92 802 2868.

E-mail address: ishihara@cstf.kyushu-u.ac.jp (T. Ishihara).

In the charge, Fe oxide is reduced with H₂ generated by steam electrolysis, and oxygen is evolved to the air from air electrode. Large advantage of this Fe–air battery over SOFC is the larger energy density of Fe than H₂ in terms of volume of fuel, because fuel can be stored as solid in Fe. Theoretical capacity of H₂–air cell with 1 atm of H₂ is 846 mAh l⁻¹. On the other hand, theoretical capacity of Fe–air cell is 10 kAh l⁻¹. The capacity of the Fe–air battery is strongly dependent on the oxidation state of Fe, which is determined by the temperature and the oxygen partial pressure [14]. In our previous work, a cermet anode was investigated for Fe–air battery operation at 873 K [11]. However, the redox cycle stability was not sufficient due to reoxidation and aggregation of the anode at 873 K. Degradation by reoxidation of the anode is a common issue that needs to be overcome in conventional SOFC technology. Many studies on reoxidation behavior in SOFCs have been reported [15–17]. Ju et al. reported the effect of the SOFC operating temperature on the electrochemical reoxidation behavior using a LaGaO₃ based film electrolyte attached to a Ni–Fe metal substrate, and the cell exhibited much less degradation by reoxidation of the anode at lower operating temperatures because volume changes of the anode were suppressed [15]. Therefore, in the Fe–air battery, lower operating temperature would also be required to improve the redox cycle stability of the anode. In addition, from the viewpoint of usability as a battery for EVs, lower operating temperatures would be preferable. The present work shows the effect of operation temperature on the redox cycle stability and discharge performance of an Fe–air rechargeable battery with a LaGaO₃ based electrolyte and a Ni-based anode.

2. Experimental

In this study, two types of the cell structure (Planar-type cell and Tubular-type cell) were used. Most of the experimental were performed by using planar-type cell because of easily setup. On the other hand, more tight gas sealing is required for electrochemical charge and discharge and so we used tubular type cell because of easily gas sealing achieved. Details of the experimental setup for planar-type cell have been previously reported [9]. An electrolyte supported planar single cell (17 mm in diameter and 0.3 mm thick) was used to study the operating temperature dependency and the La_{0.9} Sr_{0.1} Ga_{0.8} Mg_{0.2} O₃ (LSGM) electrolyte was prepared by the conventional solid state method using La₂O₃, SrCO₃, Ga₂O₃, MgO as starting materials [18]. The starting powder mixture was calcined at 1273 K for 6 h and then pressed into disks which were then sintered at 1773 K for 6 h. The LSGM disks were polished to a thickness of 0.3 mm. A cermet anode of Ni–Fe combined with Ce_{0.6}Mn_{0.3}Fe_{0.1}O₃ (CMF) was used as the anode material. Ni–Fe (90:10, w/w) was synthesized by loading Fe(NO₃)₃·9H₂O on NiO in aqueous solution. The obtained powder was calcined in air at 873 K to decompose the nitrate solution and produce the oxides. Ce_{0.6}Mn_{0.3}Fe_{0.1}O₃ (CMF) was synthesized by the evaporation method using an aqueous solution of Ce(NO₃)₃·6H₂O, Mn(NO₃)₃·6H₂O, and Fe(NO₃)₃·9H₂O. The obtained powder was calcined in air at 1473 K. Ni–Fe and CMF were mixed by grinding to produce the cermet of Ni–Fe with CMF. Ba_{0.6}La_{0.4}CoO₃ (BLC) was used as the cathode material and was prepared by the solid state reaction method. The anode and cathode powders were applied to 5 mm diameter areas of each respective face of the LSGM disk using a screen printing method followed by calcination at 1373 K for 30 min. The prepared planar single cell was set between Al₂O₃ tubes using molten Pyrex glass as a gas sealant. Fe oxide powder (50 mg) was set under the planar SOFC on the anode side with quartz wool. After heating the cell to the operating temperature, humidified hydrogen (3 vol% H₂O) was supplied to the anode side to reduce the Ni–Fe oxides in the anode and the Fe oxide powder to the metallic state. After reduction for

2 h, the gas in the Fe chamber was diluted (3% H₂O, 87.3% N₂, 9.7% H₂) and then separated from the gas supply line by two stop valves. The discharge capacity of the cell was measured using the 4-probe method under application of a constant current (5 mA cm⁻²). In the case of the planar cell, charging was performed by reduction with H₂ flow after discharge, and thus, cycle testing was performed by electrochemical discharge and chemical charge.

A tubular cell was produced using an extruded LSGM tube (1 mm thick, 13 mm diameter, and 9.7 mm long, 12.9 ml of volume; Nippon Tokushu Kogyo Co., Ltd.) for cyclic electrochemical charge–discharge measurements at 773 K. Electrode materials were the same with the case of planner type cell mentioned above. Pastes for electrode were painted on the inside (anode) and outside (cathode) of LSGM tube. Then, foam Ag and Ag wire were applied for the current corrector and lead wire, respectively. The effective electrode area was 4 cm² and the applied constant current for charge–discharge measurement was 5 mA (1.25 mA cm⁻²). The gas condition for the cell performance measurement was same as those for the planar cell, and it is noted that H₂ gas initially contained in the LSGM tube is 12.87 ml (0.02 mmol), which is corresponded to 1.06 mAh. 50 mg of Fe powder (Fe₃O₄, 0.22 mmol) was inserted in a small alumina tube, and the alumina tube was set in the LSGM electrolyte tube. AC impedance measurements were performed using a potentiostat (Solartron 1287) and frequency response analyzer (Solartron 1260) combined with a computer. The impedance spectra were measured in the frequency range from 0.1 to 10⁵ Hz with a signal amplitude of 10 mV. The electrode morphology was observed using scanning electron microscopy (SEM; Keyence VE-7800). Particle size distribution of anode was measured by Laser Scattering Particle Size Distribution Analyzer (LA920, HORIBA). Oxidation rate of Fe by steam was analyzed with TG-DTA (Thermo Plus 2, Rigaku). Fe powder was inserted in tube type furnace followed by oxidation in H₂O at 973 K, 873 K, and 773 K under 2.8 vol% H₂O–N₂ flow condition at 50 ml min⁻¹.

3. Results and discussion

3.1. Effect of operating temperature on the discharge performance

Fig. 1 shows the discharge curves of Fe–air cell for several cycles with different operating temperatures. A higher discharge potential was achieved at 773 K than that at 973 K, and the potential plateau was extremely flat, whereas the operating potential observed at 973 K gradually decreased. The cycle stability and discharge capacity was also increased by operating at 773 K, and the discharge

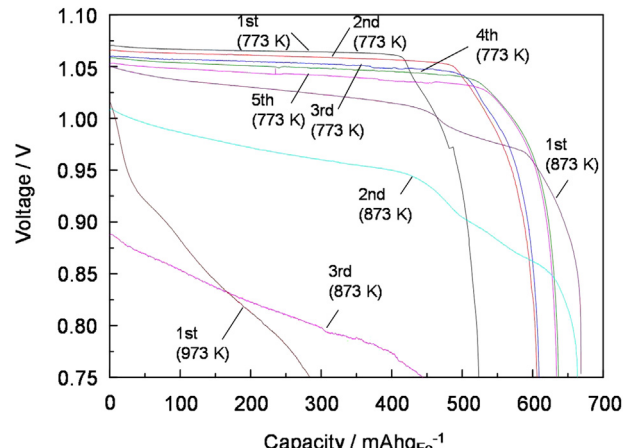


Fig. 1. Discharge curves of Fe–air cell operated at 773, 873, and 973 K.

potential was 1.04 V, even at the fifth cycle. On the other hand, at 973 K, a second discharge could not be performed because the internal resistance was too large after the first discharge. It should also be noted that the capacity at 773 K was increased with increasing cycle number. The reasons for this phenomenon are discussed later. The discharge capacity was lower than we have previously reported, because of the lower current density [12]. In the conventional battery, discharge capacity decreases with increasing current density. However, in our previous study, it was found that the higher discharge current density (=faster oxidation rate of Fe powder) leads to the larger discharge capacity and also superior cycle stability. This could be related with sustaining porosity and small particle size of Fe powder under high oxidation condition. This is one of the interesting property of this battery. After discharge was cut off, the open circuit potential was monitored and the oxygen partial pressure in the Fe chamber (anode side) was estimated from the Nernst equation. The observed P_{O_2} in the cell after cut off at 0.75 V were $10^{-24.4}$ atm (773 K), $10^{-22.3}$ atm (873 K), and $10^{-21.1}$ atm (973 K). Therefore, in all cases, the stable iron oxide formed is Fe_3O_4 , according to the Keringum diagram [14]. This discussion is based on the thermodynamic equilibrium state. It is also noted that XRD result reveals that iron oxide after the discharge is assigned to the Fe_3O_4 . There may be two main possibilities for the high discharge potential achieved at 773 K. One is related to the particle size of the Fe powder, and the second is related to the activity of the anode, which is dependent on the state of Ni–Fe aggregation. This may be related to the surface area of the anode because aggregation is more pronounced at higher operating temperatures. On the other hand, the rate of H_2 formation from Fe powder should be discussed further because the H_2 concentration is an important factor influencing the discharge potential, as reported previously [12].

Fig. 2(a) shows impedance plots for the anode before discharge in a H_2 flow. In a H_2 flow, the effect of H_2 formation by Fe oxidation can be ignored because Fe is almost the metallic state and H_2 is only supplied by flowed H_2 , not from Fe, and therefore, we can discuss only the anodic performance. The anodic semicircle at 773 K was smaller than that at 973 K, which suggests that Ni–Fe in the anode is easily aggregated at higher temperature. Therefore, the anode would be expected to be more stable at 773 K. **Fig. 2(b)** shows impedance plots for the anode in the Fe–air cell after discharge to

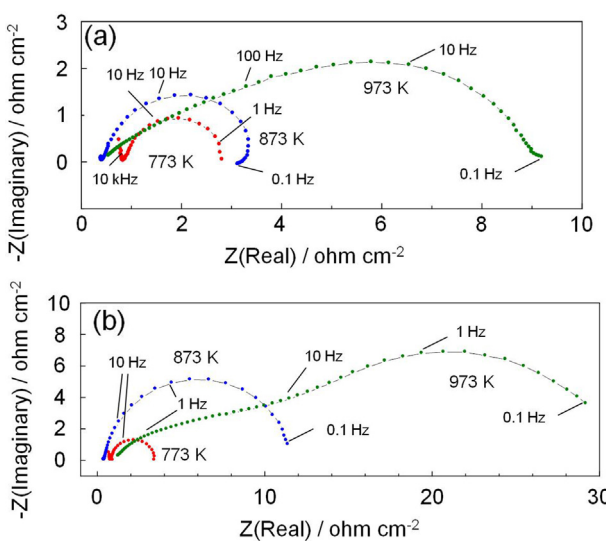


Fig. 2. Impedance plots for the anode side. (a) H_2 –air cell (H_2 flow at the anode), and (b) Fe–air cell after discharge to $100 \text{ mAh g}_{\text{Fe}}^{-1}$.

100 mAh g_{Fe}^{-1} . When the operating temperature was 973 K, the polarization resistance of the Fe–air battery was much larger than that of the cell with H_2 flow as shown in **Fig. 2(a)**. On the other hand, when the operating temperature was 773 K, the polarization resistance of the Fe–air battery was similar to that of the cell with H_2 flow. One reason for the small polarization resistance of Fe–air battery operated at 773 K is the high activity of the anode because of the suppressed aggregation.

Thermogravimetric-differential thermal analysis (TG-DTA) measurements were performed to examine the effect of the H_2 formation rate from Fe powder. **Fig. 3** shows TG curves for the oxidation of metallic Fe at various temperatures. Oxidation was performed using 3% H_2O in N_2 at 50 mL min^{-1} , and oxidation/reduction was performed at the same temperature. When the oxidation temperature was 773 K, the weight sharply increased and then plateaued after 5 min. On the other hand, when the redox temperature was 973 K, there were some stages of weight change. The first rapid change in weight was small (ca. 1 mg) at 973 K, which was not observed at lower temperature. During high temperature Fe oxidation, there are two possible rate-limiting steps; chemical reaction at the surface and the diffusion of consistent ions in the oxide scale (bulk oxidation) [12,19]. Therefore, the oxidation stages observed at 973 K (**Fig. 3**) can be assigned to oxidation of the surface and the bulk, which occurred before and after ca. 10 min, respectively. It can be concluded that the high oxidation rate of Fe at 773 K is caused by the suppressed aggregation of Fe powder, which may cause a small diffusion overpotential. Therefore, the second reason for the small polarization resistance observed at 773 K is H_2 formation rate from Fe in addition to the suppressed aggregation of Ni–Fe anode at 773 K as discussed.

3.2. Cycle stability

The discharge capacity increased with increasing cycle number at 773 K; therefore, the mechanism for this was investigated. SEM images of the Fe powder after the first reduction and after the fifth discharge are shown in **Fig. 4**. The particle size before and after the redox cycle was similar, which indicates that no significant aggregation of Fe occurred at 773 K. However, the microstructure was much different. After the 1st reduction, the Fe particles were dense, but became porous after the fifth discharge. This result indicates that the pores in the oxide may be formed due to void formation and/or compressive stress during the redox cycle as reported [12,19].

To reveal the difference in the hydrogen formation from Fe powder with the redox cycle number, the redox cycle was

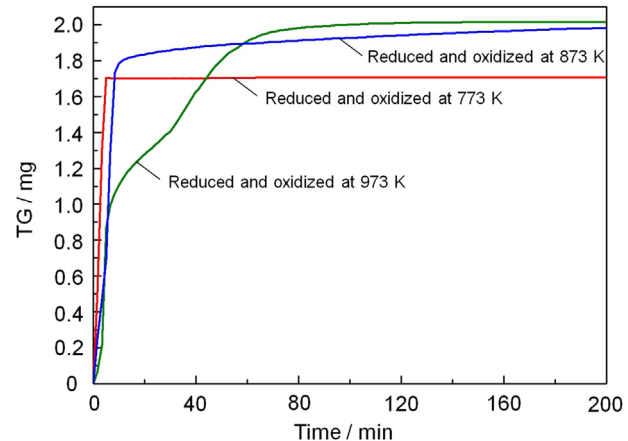


Fig. 3. TG curves for Fe powder oxidation after reduction at various temperatures.

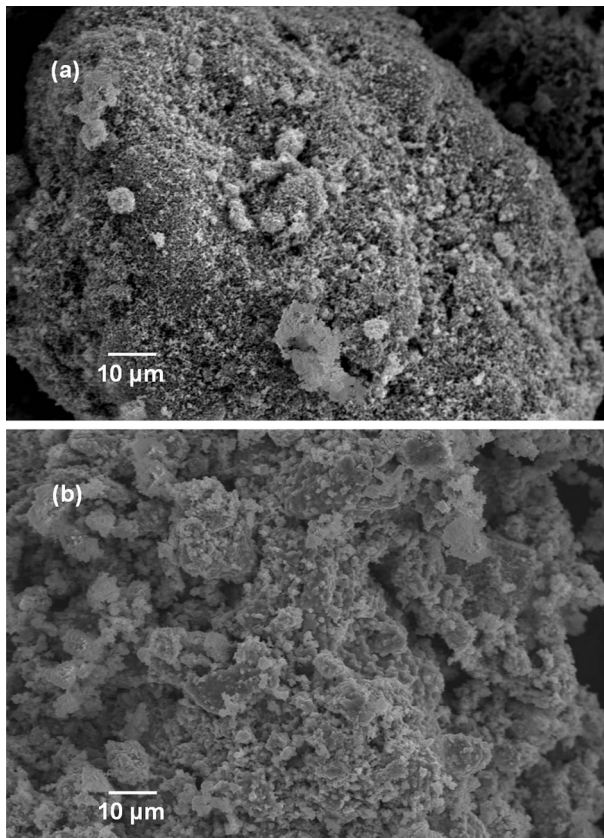


Fig. 4. SEM images of Fe powder (a) after reduction at 773 K, and (b) after discharge for 5 cycles at 773 K.

conducted five times and then TG-DTA measurement was performed. TG oxidation curves for Fe after a single reduction and after the fifth cycle are shown in Fig. 5. A much larger weight change during initial oxidation was observed for the Fe powder treated with a redox cycle, which suggests that the porous structure formed by redox treatment is highly effective for gas diffusion and results in a small diffusion overpotential. Therefore, the larger discharge capacity in the fifth cycle at 773 K than that at the first cycle is assigned to the formation of the porous structure during the redox cycles.

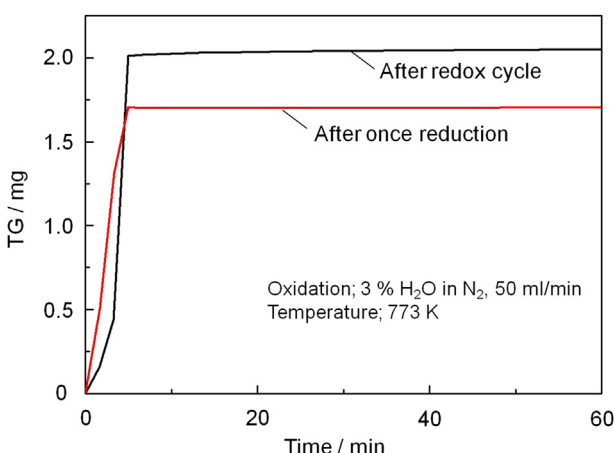


Fig. 5. TG curves for the oxidation of Fe powder after one time reduction and five times reduction. Reduction and oxidation were conducted at 773 K.

Fig. 6 shows impedance plots for the anode during cycle testing at various operating temperatures with 3% H_2O in H_2 supplied as the fuel. When the operating temperature was higher than 873 K, there was a significant increase in the semicircle and the ohmic resistance at the high frequency intercept with cycle number. The reason for increase in ohmic resistance seems to be explained by the decreased contact of the anode due to the aggregation and sintering easily occurred during redox cycle at higher temperature. This was also confirmed by SEM observations. In contrast, the ohmic loss and overpotential at 773 K were stable, compared with those at 973 K. Therefore, when the cell was operated at 773 K, the discharge capacity and the potential plateau were maintained over 5 cycles.

Fig. 7(a), (b), and (c) shows SEM images of the anode after discharge at 773, 873, and 973 K, respectively. Aggregation of the anode became more significant with increased operating temperature. To confirm the aggregation of anode more quantitatively, particle size distribution was measured. Fig. 8 shows the particle size distribution of anode after redox cycle. Larger particle size of anode was observed with operating at higher temperature. Therefore, the higher cycle stability at 773 K can be explained by the prevention of anode re-oxidation, which results in the prevention of aggregation and maintains a small overpotential. As a result, the reason for the excellent cycle stability obtained at 773 K was assigned to the fine particles of the Ni anode during discharge.

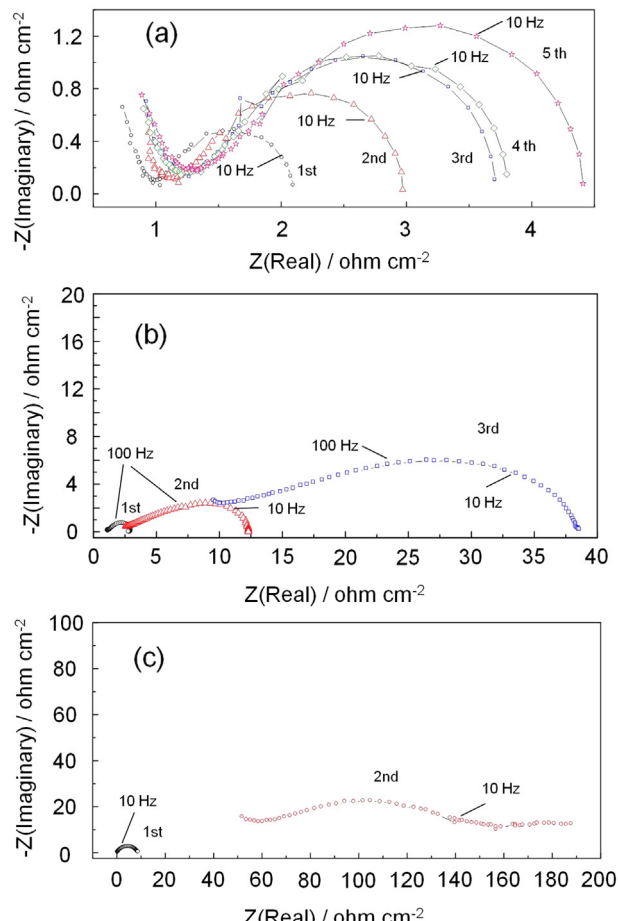


Fig. 6. Impedance plots for the anode during the cycle tests at (a) 773, (b) 873, and (c) 973 K. 100 mL min^{-1} of O_2 and H_2 was flowed to the cathode and anode, respectively, during the measurement.

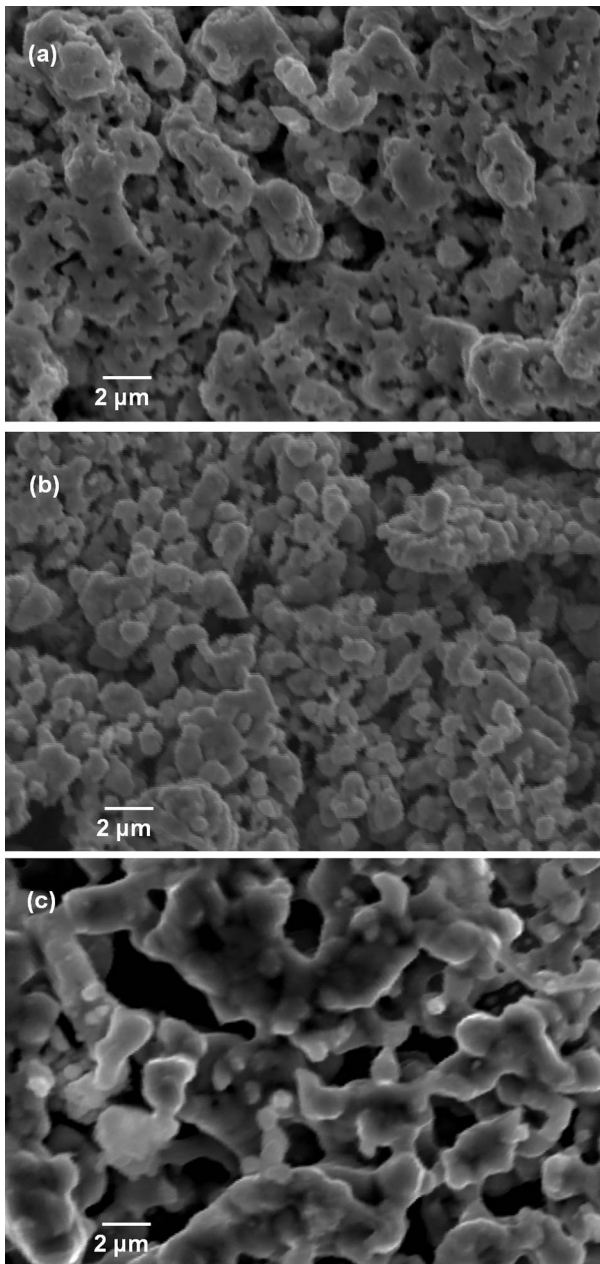


Fig. 7. SEM images of the anode after a) the fifth discharge at 773 K, b) the third discharge at 873 K, and c) first discharge at 973 K.

3.3. Electrochemical charge–discharge cycle using tubular type LSGM electrolyte

Electrochemical charge–discharge is more suitable as secondary battery than chemical charge with H₂ flow considering small space, low cost, and infrastructure. To confirm the electrochemical reversibility of the Fe–air rechargeable battery when operated at 773 K, electrochemical charge–discharge cycling was investigated. For prolonged charge–discharge cycling, a gas tight cell is required; therefore, a tubular type LSGM was used for the electrolyte. Fig. 9(a) shows charge–discharge curves for the Fe–air rechargeable battery with the tubular type cell at 773 K. At the first charge or discharge cycle, the capacity was limited to 445 mAh g_{Fe}⁻¹. It is noted that the original H₂ gas contributed to the charge/discharge capacity which is calculated from the volume of LSGM tube is 1.06 mAh. However,

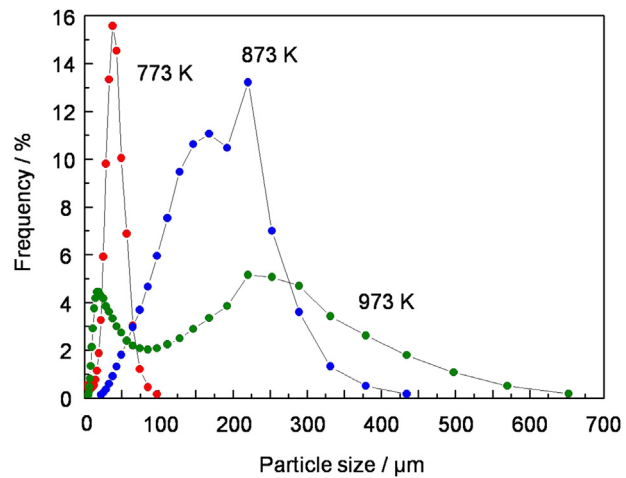


Fig. 8. Particle size distribution of anode after redox cycle.

in actual, we could obtain the 21.1 mAh of capacity in each discharge capacity. Therefore, original H₂ gas contributed to the charge/discharge capacity is only 5% at largest, and so the observed discharge capacity was mainly based on the redox of Fe. A flat charge/discharge potential could be observed for 30 cycles at 773 K. The energy efficiency for charge/discharge was sustained between 80 and 90% during the cycle test, as shown in Fig. 9(b). This result suggests that this new type of Fe–air battery has excellent rechargeable performance and a high energy density (ca. 450 Wh kg_{Fe}⁻¹) when operated at 773 K. This is a much higher energy

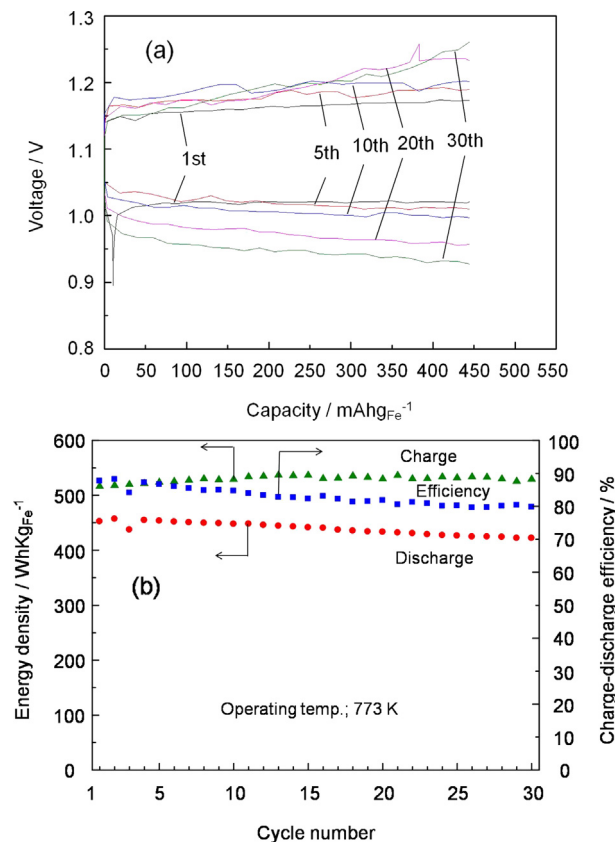


Fig. 9. (a) Charge–discharge curves and (b) cycle properties for the Fe–air rechargeable battery with a tubular type of LSGM electrolyte operated at 773 K.

density than that for a Li-ion battery (250 Wh kg^{-1} theoretical maximum) and represents sufficient performance for use as a next generation device for energy grid applications. On the other hand, volumetric capacity calculated from the volume of the LSGM tube is 1640 mAh l^{-1} for the present cell, because dead volume is still very large (12.87 ml) and limited amount of Fe powder. However, even the large dead volume, current volumetric capacity is much higher than the theoretical capacity of H_2 -air cell with 1 atm of H_2 (846 mAh l^{-1}). We may be able to increase the volumetric capacity to a theoretical one ($10,837 \text{ Wh l}^{-1}$) because excess amount of dead volume just disturb the $\text{H}_2/\text{H}_2\text{O}$ diffusion and theoretically smaller volume is preferable for increasing rate property.

This study has demonstrated that low-temperature operation of the Fe–air battery allows a high performance to be achieved. Future works include lower temperature operation, for example 673 K and 573 K. To be achieved low temperature operation, application of thin film electrolyte and more active Fe powder for H_2 generation by approaching of control the structure and adding catalyst are essentially requested. These are now under study, and it will be reported in future.

4. Conclusion

The effect of operating temperature on the discharge potential and cycle stability of an Fe–air battery using a LaGaO_3 electrolyte was investigated at temperatures from 773 to 973 K. The highest discharge potential (1.07 V) was achieved when the operating temperature was 773 K. A detailed analysis of the internal resistance in the H_2 flow system showed that the anodic overpotential at 773 K was lower than that at higher temperatures (973 and 873 K) because aggregation of anode was suppressed. This is a one reason for the high discharge potential during operation at 773 K. TG analysis also indicated that surface oxidation of the Fe powder and a high rate of H_2 formation could be achieved at 773 K because the aggregation of Fe was suppressed at lower temperature. The increased discharge capacity with cycle number at 773 K can be explained by the formation of a porous structure in the Fe powder particles during redox cycling, which results in improved gas diffusion and thus high usage efficiency for Fe. The cycle stability of the anode was also much better during operation at 773 K than at 973 K. Aggregation of Ni–Fe during the redox cycle was not significant when the cell was operated at 773 K, so that stable cycle stability was achieved.

Electrochemical charge–discharge cycle tests revealed that an Fe–air battery operated at 773 K can exhibit reasonably high cycle stability with a high energy density and energy efficiency for 30 cycles. Compared with the use of yttria-stabilized zirconia (YSZ) as an electrolyte, the application of LSGM, which is a superior oxide ion conductor, enables low temperature operation at 773 K, and this is effective at decreasing the energy required to maintain the operating temperature.

Acknowledgments

This study was financially supported in part by the Advanced Low Carbon Technology Research and Development Program (ALCA) of the Japan Science and Technology Agency. The authors also acknowledge the financial support from a Grant-in-Aid for Scientific Research(S), No. 24226016. I²CNER are supported by the WPI Program of the Ministry of Education, Sports, Culture, Science, and Technology (MEXT), Japan.

References

- [1] H. Chen, T. Ngoc Cong, W. Yang, C. Tan, Y. Li, Y. Ding, *Prog. Nat. Sci.* 19 (2009) 291–312.
- [2] B. Dunn, H. Kamath, J.M. Tarascon, *Science* 18 (2011) 928–935.
- [3] S.A. Freunberger, Y. Chen, Z. Peng, J.M. Griffin, L.J. Hardwick, F. Bardé, P. Novák, P.G. Bruce, *J. Am. Chem. Soc.* 133 (2011) 8040–8047.
- [4] K.M. Abraham, Z. Jiang, *J. Electrochem. Soc.* 143 (1996) 1.
- [5] D. Capsoni, M. Bini, S. Ferrari, E. Xuatarone, P. Mustarelli, *J. Power Sources* 220 (2013) 254.
- [6] U. Sahapatsombut, H. Cheng, L. Scott, *J. Power Sources* 243 (2013) 409.
- [7] X. Zhao, N. Xu, X. Li, T. Gong, K. Huang, *RSC Adv.* 2 (2012) 10163–10166.
- [8] N. Xu, X. Li, X. Zhao, J.B. Goodenough, K. Huang, *Energy Environ. Sci.* 4 (2011) 4942–4946.
- [9] A. Inoishi, S. Ida, S. Uratani, T. Okano, T. Ishihara, *Phys. Chem. Chem. Phys.* 14 (2012) 12818–12822.
- [10] A. Inoishi, Y.W. Ju, S. Ida, T. Ishihara, *J. Power Sources* 229 (2013) 12–15.
- [11] A. Inoishi, S. Ida, S. Uratani, T. Okano, T. Ishihara, *RSC Adv.* 3 (2013) 3024–3030.
- [12] A. Inoishi, Y. Okamoto, Y.W. Ju, S. Ida, T. Ishihara, *RSC Adv.* 3 (2013) 8820–8825.
- [13] A. Inoishi, Y.W. Ju, S. Ida, T. Ishihara, *Chem. Commun.* 49 (2013) 4691–4693.
- [14] K.C. Condie, *Geol. Soc. Am. Bull.* 74 (1964) 361.
- [15] Y.W. Ju, S. Ida, T. Inagaki, T. Ishihara, *J. Power Sources* 195 (2011) 6062–6069.
- [16] T. Hatae, Y. Matsuzaki, S. Yamashita, Y. Yamazaki, *Solid State Ionics* 180 (2009) 1305–1310.
- [17] M. Ettler, H. Timmermannb, J. Malzbendera, A. Weber, N.H. Menzler, *J. Power Sources* 195 (2010) 5452–5467.
- [18] T. Ishihara, H. Matsuda, Y. Takita, *J. Am. Chem. Soc.* 116 (1994) 3801.
- [19] T. Maruyama, M. Ueda, *J. Korean Ceram. Soc.* 47 (2010) 8–18.